

# Predictable Patterns of Wintertime Surface Air Temperature in Northern Hemisphere and Their Predictability Sources in the SEAS5

HONGDOU FAN,<sup>a,b</sup> LIN WANG,<sup>a,b</sup> YANG ZHANG,<sup>c</sup> YOUMIN TANG,<sup>d</sup> WANSUO DUAN,<sup>e</sup> AND LEI WANG<sup>a</sup>

<sup>a</sup> Center for Monsoon System Research, Institute of Atmospheric Physics, Chinese Academy of Sciences, Beijing, China

<sup>b</sup> College of Earth and Planetary Sciences, University of Chinese Academy of Sciences, Beijing, China

<sup>c</sup> School of Atmospheric Sciences, Nanjing University, Nanjing, China

<sup>d</sup> Environmental Science and Engineering, University of Northern British Columbia, Prince George, British Columbia, Canada

<sup>e</sup> State Key Laboratory of Numerical Modeling for Atmospheric Sciences and Geophysical Fluid Dynamics, Institute of Atmospheric Physics, Chinese Academy of Sciences, Beijing, China

(Manuscript received 13 July 2020, in final form 3 September 2020)

**ABSTRACT:** Based on 36-yr hindcasts from the fifth-generation seasonal forecast system of the European Centre for Medium-Range Weather Forecasts (SEAS5), the most predictable patterns of the wintertime 2-m air temperature (T2m) in the extratropical Northern Hemisphere are extracted via the maximum signal-to-noise (MSN) empirical orthogonal function (EOF) analysis, and their associated predictability sources are identified. The MSN EOF1 captures the warming trend that amplifies over the Arctic but misses the associated warm Arctic-cold continent pattern. The MSN EOF2 delineates a wavelike T2m pattern over the Pacific–North America region, which is rooted in the tropical forcing of the eastern Pacific-type El Niño–Southern Oscillation (ENSO). The MSN EOF3 shows a wavelike T2m pattern over the Pacific–North America region, which has an approximately 90° phase difference from that associated with MSN EOF2, and a loading center over midlatitude Eurasia. Its sources of predictability include the central Pacific-type ENSO and Eurasian snow cover. The MSN EOF4 reflects T2m variability surrounding the Tibetan Plateau, which is plausibly linked to the remote forcing of the Arctic sea ice. The information on the leading predictable patterns and their sources of predictability is further used to develop a calibration scheme to improve the prediction skill of T2m. The calibrated prediction skill in terms of the anomaly correlation coefficient improves significantly over midlatitude Eurasia in a leave-one-out cross-validation, implying a possible way to improve the wintertime T2m prediction in the SEAS5.

**KEYWORDS:** Climate prediction; ENSO; Snow cover; Sea ice; Surface temperature

## 1. Introduction

A reliable numerical weather forecast is usually limited to about two weeks (Bauer et al. 2015; Simmons and Hollingsworth 2002) because of the chaotic dynamics of atmospheric circulation (Lorenz 1963). The latter is also the main source of uncertainties or noises in seasonal climate predictions. In contrast, the existence of slowly varying atmospheric boundaries such as sea surface temperature (SST), sea ice, and snow cover gives rise to the feasibility of seasonal predictions (e.g., Charney and Shukla 1981; Doblas-Reyes et al. 2013; Kim et al. 2012) because they can alter the likelihood of residence in atmosphere attractors and thereby constrain the behaviors of the atmosphere on monthly and longer time scales (Palmer 1993). Accordingly, the changes in the atmosphere that are associated with these external factors could be regarded as potentially predictable, whereas the remaining part of changes be regarded as potentially unpredictable in seasonal predictions.

Seasonal climate predictability has been widely investigated regarding its spatial pattern and predictability sources using dynamical models. Various approaches, such as signal-to-noise metrics, have been proposed to quantify the seasonal predictability (Rowell 1998). However, assessing seasonal predictability using only one snapshot map makes it difficult to detect

the predictability sources because it lacks information on temporal evolutions. Besides, certain spatial or temporal structures may still be predictable with an optimized method despite the low predictability in some areas (e.g., middle and high latitudes). These inadequacies inspired a unified framework for investigating predictability based on information theory, in which the key approach is the maximized signal-to-noise (MSN) empirical orthogonal function (EOF) analysis (Allen and Smith 1997; DelSole and Tippett 2007). This framework provides reliable estimations of predictability by considering nonlinear factors, and it is convenient to explore the spatial and temporal structures of predictability through which the involved mechanism can be revealed. For example, Tang et al. (2014, 2015) extracted the first and second predictable patterns of the North American surface air temperature via the MSN EOF analysis and attributed them to El Niño–Southern Oscillation (ENSO) and global warming, respectively. They further suggested that the first predictable pattern is inherent to the most predictable patterns of the SST and 500-hPa geopotential height. Scholars also use the MSN EOF analysis to investigate the predictable patterns of monsoon precipitation (e.g., Liang et al. 2008; Zuo et al. 2013), the tropical Indian Ocean SST (e.g., Wu and Tang 2019; Zhu et al. 2015), and the tropical Atlantic Ocean SST (e.g., Huang 2004), among others, confirming the efficiency of the methodology.

Skillful seasonal prediction is crucial for Eurasia, where the population density is high, and the natural hazard is frequent.

Corresponding author: Lin Wang, wanglin@mail.iap.ac.cn

DOI: 10.1175/JCLI-D-20-0542.1

© 2020 American Meteorological Society. For information regarding reuse of this content and general copyright information, consult the AMS Copyright Policy ([www.ametsoc.org/PUBSReuseLicenses](http://www.ametsoc.org/PUBSReuseLicenses)).

In contrast to the climate of the Pacific–North America (PNA) region that is tightly related to ENSO (e.g., Horel and Wallace 1981; Zhu et al. 2013, 2017; Tang et al. 2014, 2015), the Eurasian climate is less influenced by ENSO on the interannual time scale because of the complex processes and nonstationary footprint of ENSO (e.g., Ineson and Scaife 2008; Kumar et al. 1999; Wu and Wang 2002; Jia et al. 2017; Wang et al. 2008; Gong et al. 2019; Xie et al. 2016). Meanwhile, the involvement of other active boundary forcing such as snow cover and sea ice (e.g., Cohen and Fletcher 2007; Cohen et al. 2014; Zuo et al. 2011, 2015) further increases the complexity and uncertainty of the seasonal prediction over Eurasia. Moreover, it remains unclear what the predictable patterns of the Eurasian climate and their sources are, motivating a careful investigation via the state-of-the-art seasonal forecast systems. In this study, the leading predictable patterns of the wintertime surface air temperature in the whole extratropical Northern Hemisphere, with the emphasis on the Eurasian region, and their predictability sources are investigated based on the outputs of the latest seasonal forecast system of the European Centre for Medium-Range Weather Forecasts (ECMWF). Given the above understanding, a calibration scheme for seasonal prediction is proposed, which turns out to evidently improve the prediction skill of surface air temperature over the Eurasian region.

This paper is laid out as follows. Section 2 describes the datasets and methodologies used in this study. Sections 3 and 4 identify the most predictable pattern of surface air temperature in the extratropical Northern Hemisphere and their predictability sources, respectively. Section 5 develops a calibration scheme to improve the prediction skill of surface air temperature by reinforcing the information of the leading predictable patterns. Finally, section 6 concludes the key findings and discusses some remaining issues.

## 2. Data and methods

The retrospective seasonal forecast (hindcast) data used in this work are from the fifth-generation seasonal forecast system (SEAS5; Johnson et al. 2019) of the ECMWF, which consists of 25 ensemble members for the 36-yr hindcast period 1981–2016. The data have a horizontal resolution of  $1^\circ \times 1^\circ$  and 11 vertical pressure levels extending from 925 to 10 hPa. As a state-of-the-art seasonal forecast system, the SEAS5 is a fully coupled general circulation models initialized on the first day of every month and integrated continuously for seven months (Johnson et al. 2019). It uses the Integrated Forecast System (IFS) atmospheric model cycle 43r1 as its atmospheric component and the Nucleus for European Modeling of the Ocean (NEMO) model version 3.4.1 as its oceanic component. It also includes a prognostic sea ice model, the Louvain-la-Neuve sea ice model version 2 (LIM2), under the NEMO modeling framework to improve the land–ice interactions. The atmosphere, ocean, snow, sea ice, and other land fields are perturbed using an ensemble of data assimilations to represent uncertainty in the initial state and ensemble spread. Compared with its predecessor, System 4, the SEAS5 shows many important improvements, such as a better ENSO prediction skill. More details can be found in Johnson et al. (2019) and the SEAS5 user guide via <https://www.ecmwf.int/sites/default/>

[files/media/library/2017-10/System5\\_guide.pdf](https://www.ecmwf.int/sites/default/files/media/library/2017-10/System5_guide.pdf). This study uses the monthly mean hindcast data initialized on 1 November, which is the most informative for the winter season. The use of the one-month lead hindcasts is because it can balance between incorporating the latest observed information into the seasonal forecast system and guaranteeing enough time to take precautions for the coming season.

Several reanalysis and observational datasets are used to evaluate and verify the results of hindcasts. The atmospheric data are the monthly mean atmospheric reanalysis data from the ERA-Interim dataset (Dee et al. 2011), which has a horizontal resolution of  $1^\circ \times 1^\circ$  and 37 vertical pressure levels from 1000 to 1 hPa. The snow depth data are also from the ERA-Interim dataset. The oceanic data are the observed monthly mean SST and sea ice concentration (SIC) data from Hadley Centre Sea Ice and Sea Surface Temperature dataset, version 1 (HadISST1; Rayner et al. 2003), which has a  $1^\circ \times 1^\circ$  resolution and spans from 1870 to the present. These data are referred to as “observation” hereafter.

This study focuses on the boreal winter that is defined as the mean of December, January, and February. Climatology is defined as the 36-yr (1981–2016) mean of the 25-member ensemble mean in the SEAS5 and as the 36-yr mean in observational and reanalysis datasets. The winter of 1981 refers to the 1981/82 winter. The anomaly is calculated by removing the climatology from the raw data. The two-tailed Student’s  $t$  test is used to evaluate the significance of regression, correlation, linear trend, and the differences between two linear trends (Santer et al. 2000). The Fisher  $z$  transformation is used to evaluate the significance of differences between two correlation coefficients (Conlon and Thomas 1993).

The most predictable patterns were extracted by applying the MSN EOF (Allen and Smith 1997; DelSole and Tippett 2007; Tang et al. 2014) to the hindcast data from the SEAS5 as follows. The MSN EOF method assumes that the ensemble mean  $\mathbf{X}_M$  of seasonal mean anomalies  $\mathbf{X}$  can be decomposed into a forced (i.e., predictable) component  $\mathbf{X}_F$  and a random (i.e., unpredictable) component (noise)  $\mathbf{X}_R$ :

$$\mathbf{X}_M = \mathbf{X}_F + \mathbf{X}_R. \quad (1)$$

To find the optimal pattern (i.e., the leading MSN EOFs) of  $\mathbf{X}_F$ , the key procedure is to eliminate the spatial covariance of noise by transforming the internal variation into spatially white noise, known as the prewhitening transformation. In practice, this approach is realized by performing the EOF analysis to the ensemble deviations  $\mathbf{X}' = \mathbf{X} - \mathbf{X}_M$ :

$$\mathbf{C}_R = \mathbf{E}_R \mathbf{\Lambda}_R \mathbf{E}_R^T, \quad (2)$$

where  $\mathbf{C}_R$  is the covariance matrices of  $\mathbf{X}'$ ,  $\mathbf{\Lambda}_R$  is the diagonal matrix ranking the eigenvalues in decreasing order,  $\mathbf{E}_R$  is the eigenvectors, and the superscript T indicates the transpose of the matrix. The prewhitened matrix  $\mathbf{X}'_M$  can be obtained by projecting  $\mathbf{X}_M$  onto the  $k$ th highest-ranked eigenvectors  $\mathbf{E}_R^{(k)}$ :

$$\mathbf{X}'_M = n^{1/2} (\mathbf{\Lambda}_R^{(k)})^{-1} \mathbf{E}_R^{(k)T} \mathbf{X}_M, \quad (3)$$

where  $n$  is the ensemble size. Note that  $k$  should be neither too big nor too small to obtain the well-determined noise EOF space. Here  $k$  is taken as 30 after a series of experiments, consistent with

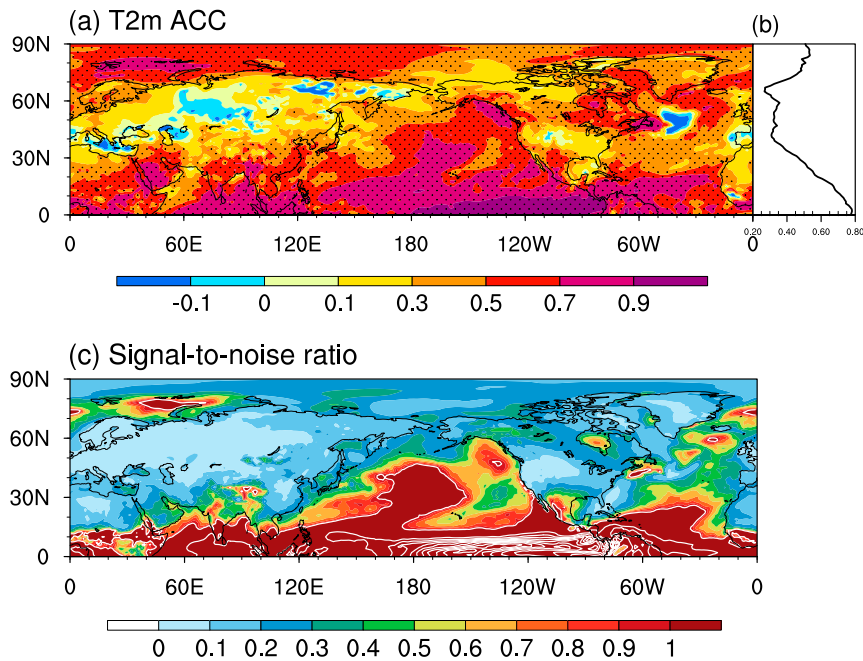


FIG. 1. (a) The ACC between observed and ensemble mean of the predicted winter mean T2m for the period 1981–2016. (b) The zonal mean of the ACC. (c) The signal-to-noise ratio of the predicted winter mean T2m, with values exceeding 1 highlighted by white contours [contour interval (CI) = 3] in (c). Dots in (a) indicate the 5% significance level based on the two-tailed Student's  $t$  test.

Huang (2004). Next, a singular value decomposition (SVD) analysis is performed on the prewhitened matrix  $\mathbf{X}'_M$ :

$$\mathbf{X}'_M = \mathbf{F}' \mathbf{v}' \mathbf{P}'^T, \quad (4)$$

where  $\mathbf{F}'$  is the left singular vectors,  $\mathbf{v}'$  is the diagonal matrix ranking the eigenvalues in the decreasing orders, and the highest-ranked right singular vector  $\mathbf{P}'$  is the optimized time series we are looking for. Finally, the most predictable pattern  $\mathbf{e}$  (i.e., the optimal pattern with maximized signal-to-noise ratio) can be obtained by projecting  $\mathbf{X}'_M$  onto the optimized time series  $\mathbf{P}'^T$ . In this procedure, the weight in space is considered (North et al. 1982), and the  $F$  test is used to evaluate the significance of the MSN EOF (Huang 2004).

### 3. Leading predictable patterns of the surface air temperature

Before analyzing the predictable patterns, we first evaluate the prediction skill of the surface air temperature in the SEAS5. Figure 1a shows the anomaly correlation coefficient (ACC) of the winter mean air temperature 2 m above the surface (T2m hereafter) between the predicted ensemble mean and observation. The ACC generally exceeds 0.3 over broad regions of the Northern Hemisphere. High ACC is located in the regions to the south of approximately 30°N, North America between 40° and 60°N, the North Pacific, and the North Atlantic. It is surprising that the ACC over the Arctic and Greenland is also high, especially over the Barents Sea, possibly due to the inclusion of the sea ice

model in the SEAS5. In contrast, the ACC over the Eurasian continent to the north of approximately 40°N is very low and even negative. This feature is also apparent in the zonal mean ACC of T2m (Fig. 1b), which shows the lowest ACC between 40° and 70°N. In addition to the linear ACC, the signal-to-noise metrics (Rowell 1998) is also used to evaluate the predictability. The signal-to-noise ratio of predicted T2m (Fig. 1c) shows a similar pattern to the ACC with high values over the tropics, subtropics, and the North Pacific (Fig. 1a). It is lower than 1 in many regions of the Arctic and North Atlantic (Fig. 1c) despite the high prediction skill (Fig. 1a). Nevertheless, a common feature between the signal-to-noise ratio and the ACC is the low predictability and skill over the Eurasian continent, especially to the north of 40°N.

Figure 2 shows the four leading predictable patterns of the winter mean T2m in the extratropical Northern Hemisphere (20°–89°N) and the time series of their corresponding principal components [MPCs hereafter;  $\mathbf{P}$  in Eq. (4)] obtained via the MSN EOF analysis. The three patterns explain 53.2%, 15.9%, and 9.3% of the total variance, respectively. They all exceed the 5% significance level based on the  $F$  test (Huang 2004), suggesting that they are significantly predictable modes. The MSN EOF1 is a monopole warming pattern in the Northern Hemisphere, and its maximum is over the Barents Sea (Fig. 2a). Its time series (MPC1) shows a prominent upward trend with some interannual variability (Fig. 2b), reminiscent of the global warming signal. These results suggest that the MSN EOF1 is likely a sign of the Arctic amplification (e.g., Fig. 2 in Cohen et al. 2014). The MSN EOF2 features warm anomalies over the

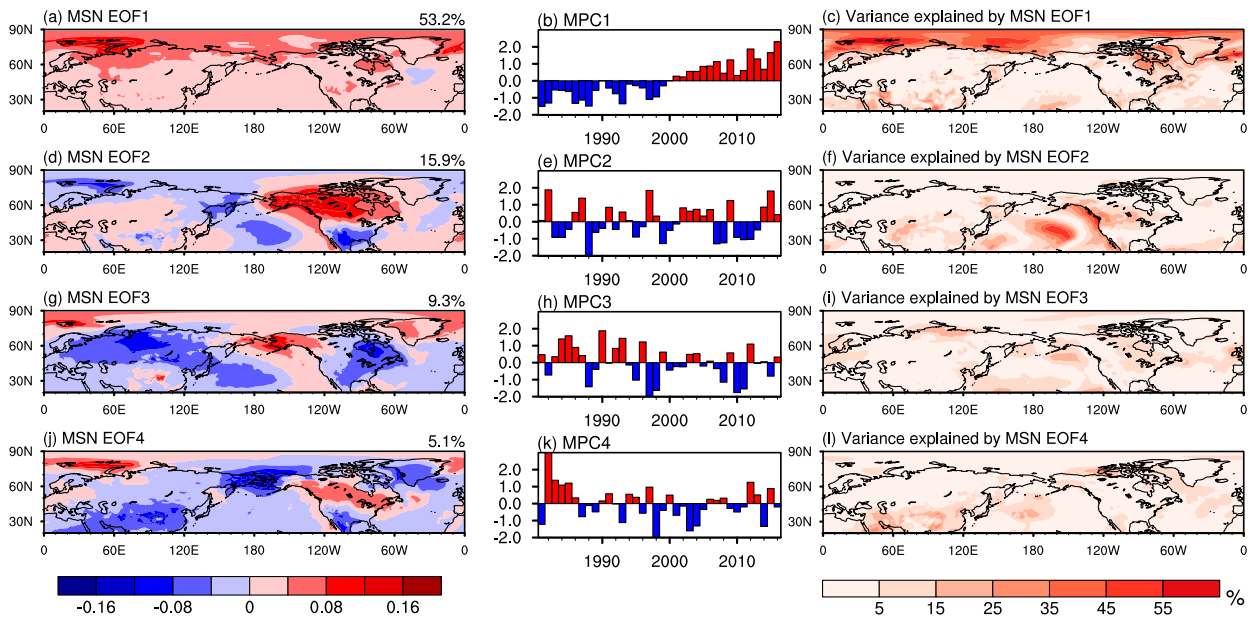


FIG. 2. (a) The MSN EOF1 of the winter mean T2m over the Northern Hemisphere ( $20^{\circ}$ – $89^{\circ}$ N) in the SEAS5. (b) The normalized principal components of the MSN EOF1 (i.e., MPC1). (c) The percent of variance (%) of the predicted T2m explained by the MSN EOF1. (d)–(f), (g)–(i), (j)–(l) As in (a)–(c), but for the MSN EOF2, MSN EOF3, and MSN EOF4, respectively. The variance explained by the MSN EOFs is denoted in the upper-right corner of (a), (d), (g), and (j).

northwestern North America and cold anomalies over the North Pacific, subtropical North America, and the Barents Sea (Fig. 2d). This pattern resembles that associated with the conventional eastern Pacific (EP) El Niño (e.g., Fig. 3 in Brönnimann 2007) and implies its plausible link to ENSO. The MSN EOF3 manifests two cold centers stretching from northern Eurasia to the subtropical central Pacific and over eastern North America, respectively, and two warm centers surrounding Alaska and Iceland (Fig. 2g). It has a third warm center over the Tibetan Plateau, but the spatial scale of this center is relatively small. The MSN EOF3 resembles the leading mode of the Eurasian surface air temperature on the interannual time scale over Eurasia (e.g., Fig. 9a in Wang et al. 2019) and the signal of the central Pacific (CP) ENSO over the PNA region (e.g., Figs. 3b and 3d in Gu and Adler 2019), implying its linkage to the CP ENSO and internal variability over Eurasia. The MSN EOF4 is characterized by cold anomalies centered over the Tibetan Plateau, the Bering Strait, the Labrador Strait, and Mexico and warm anomalies centered over the Barents Sea and midlatitude North America (Fig. 2j). This pattern does not remind us of any known climate variability, but it might be related to the forcing of the Tibetan Plateau or the changes in the Arctic sea ice because of the locations of its centers. In the next section, the atmospheric external forcing associated with the four MSN EOFs are investigated in detail to reveal the possible predictability sources of these leading predictable patterns.

#### 4. Predictability sources of the leading predictable patterns

##### a. MSN EOF1

The MSN EOF1 dominates the Arctic T2m variability and explains over 50% of the T2m variance over large areas of the

Arctic (Fig. 2c). Its monopole pattern with large loading over the Barents Sea (Fig. 2a) and the upward trend during the past decades (Fig. 2b) implies its possible origin from global warming and the associated Arctic Amplification. To confirm this inference, the long-term trend of winter mean T2m in the SEAS5 was calculated, and it shows hemispheric warming with centers over the Barents Sea and northeast North America (Fig. 3a), which is almost identical to the MSN EOF1 (Fig. 2a). The trend pattern in Fig. 3a was further projected onto the T2m in the SEAS5 to get its time evolution (not shown), which has a clear upward trend and is highly correlated to the MPC1 ( $r = 0.98$ ). These results confirm that the MSN EOF1 reflects the global warming signal in the SEAS5. A comparison of the T2m trend in the SEAS5 with that in the observation (Fig. 3b) suggests that the SEAS5 underestimates the warming trends over the Arctic and northeastern North America and fails to capture the cooling trend over central Eurasia (Fig. 3c). The failure to capture the observed warm Arctic–cold continent pattern (Overland et al. 2011), also manifested as the EOF2 of the observed T2m ( $e_2^{\text{obs}}$  hereafter) over the extratropical Northern Hemisphere (Fig. 3d), may be an essential reason for the low prediction skill of T2m over central Eurasia in the SEAS5 (Fig. 1a).

The long-term trend in the near-surface temperature during the past decades arises from the radiative forcing due to increased greenhouse gas concentrations (e.g., Stocker et al. 2013). The amplified Arctic warming has been attributed to local radiative effects, ice-albedo feedback, extratropical influences, and other processes (e.g., Chylek et al. 2009; Ding et al. 2014; Graverson et al. 2008), whereas the continental cooling may arise from the Arctic influences or the internal variability within the climate system (e.g., Cohen et al. 2014, 2020). In the SEAS5, the greenhouse gas radiative forcing is

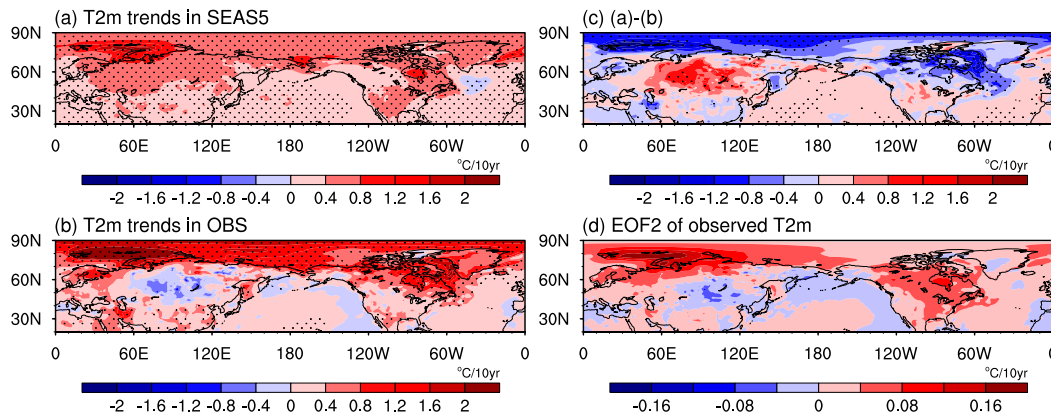


FIG. 3. Linear trends of the (a) predicted and (b) observed T2m [ $^{\circ}\text{C} (10 \text{ yr})^{-1}$ ] during winters 1981–2016. (c) Differences between (a) and (b). (d) The EOF2 of the observed winter mean T2m over the extratropical Northern Hemisphere ( $20^{\circ}$ – $89^{\circ}\text{N}$ ) derived from the period 1981–2016. Dots denote the linear trends, the difference between the linear trends and the linear regression coefficients exceed the 5% significance level in (a)–(d), respectively.

the zonally averaged seasonal varying climatology (Johnson et al. 2019). It lacks the uneven spatial distribution and the variation from year to year and thereby may cause the underestimation of the T2m trend over the Arctic. Meanwhile, the introduction of the LIM2 model introduces excess Arctic sea ice and thereby cold bias over the Arctic in the SEAS5, although it improves the skill in predicting the interannual variability in sea ice (Johnson et al. 2019). This may be another reason to underestimate the warming trend over the Arctic and thereby the cooling trend over Eurasia. Besides, the biases in the winter temperature trends may also arise from the imperfection of models in simulating the snow cover variability and the corresponding stratosphere–troposphere coupling (e.g., Cohen et al. 2012), but this is out of the scope of the current study and needs further investigation in the future.

### b. MSN EOF2

The MSN EOF2 dominates the T2m variability over the PNA region and explains approximately 50% of the T2m variance over the central North Pacific and western and central North America (Fig. 2f). Its associated T2m anomalies resemble those during the conventional EP El Niño (Fig. 3 in Brönnimann 2007) and imply its likely link to the EP ENSO. To seek its sources of predictability, the predicted winter mean SST is regressed onto the MPC2 of T2m, which shows a prominent EP El Niño pattern. The SST warming is located in the tropical central and eastern Pacific and the Indian Ocean, and the SST cooling is over the subtropical Pacific (Fig. 4a). The associated 500-hPa geopotential height anomalies manifest a PNA-like wave train emanating from the subtropical central Pacific (Fig. 4b). This wave train is equivalent barotropic (Fig. 4c), and it could induce anomalous warming over northwestern North America and cooling over the central North Pacific and southeastern North America via temperature advection (Fig. 4c). These results suggest that the predictability of MSN EOF2 is very likely rooted in the EP ENSO forcing. To further confirm this interpretation, the conventional EOF analysis was applied to the

predicted winter mean SST in the tropical Pacific ( $30^{\circ}\text{S}$ – $30^{\circ}\text{N}$ ,  $110^{\circ}\text{E}$ – $70^{\circ}\text{W}$ ). The EOF1 of predicted SST shows a conventional EP El Niño pattern (Fig. 4d), and its associated 500-hPa geopotential height anomalies (Fig. 4e) and T2m anomalies (Fig. 4f) quite resemble those associated with the MSN EOF2 of T2m (Figs. 4b,c). The correlation coefficient between MPC2 of T2m and PC1 of SST, referred to as  $\text{PC1}_{\text{SST}}$ , is 0.87, exceeding the 1% significance level. Hence, the EP ENSO is a crucial source of predictability for the T2m's MSN EOF2. This result is overall consistent with Tang et al. (2014) that ENSO's SST forcing dominates the most predictable T2m pattern over the PNA region.

In addition to the EP ENSO forcing from the tropical Pacific, the MSN EOF2 of T2m is also closely related to the wintertime snow depth over North America (not shown). The correlation coefficient between the MPC2 and the predicted area-averaged ( $40^{\circ}$ – $60^{\circ}\text{N}$ ,  $170^{\circ}$ – $60^{\circ}\text{W}$ ) snow depth index is pretty high ( $-0.77$ ). However, the regression of the wintertime T2m onto the above snow depth index after removing the ENSO signal does not show much significant signal in the PNA region. Here, the removal of the ENSO signal is realized by subtracting the regression coefficient of the predicted snow depth index onto the simultaneous predicted Niño-3.4 index from the predicted snow depth index (Wang et al. 2007; Chen et al. 2013). This result suggests that the North America snow anomalies are more like a passive response to EP ENSO rather than an independent atmospheric external forcing for the MSN EOF2 of T2m.

### c. MSN EOF3

The MSN EOF3 mainly influences the T2m variability over the North Pacific and Eurasia, and it explains approximately 25% and 15% of the T2m variance over the northwestern Pacific and central northern Eurasia (Fig. 2i), respectively. Its associated T2m anomalies are similar to those associated with the CP ENSO over the PNA region (e.g., Figs. 3b and 3d in Gu and Adler 2019). It is directly induced by a barotropic

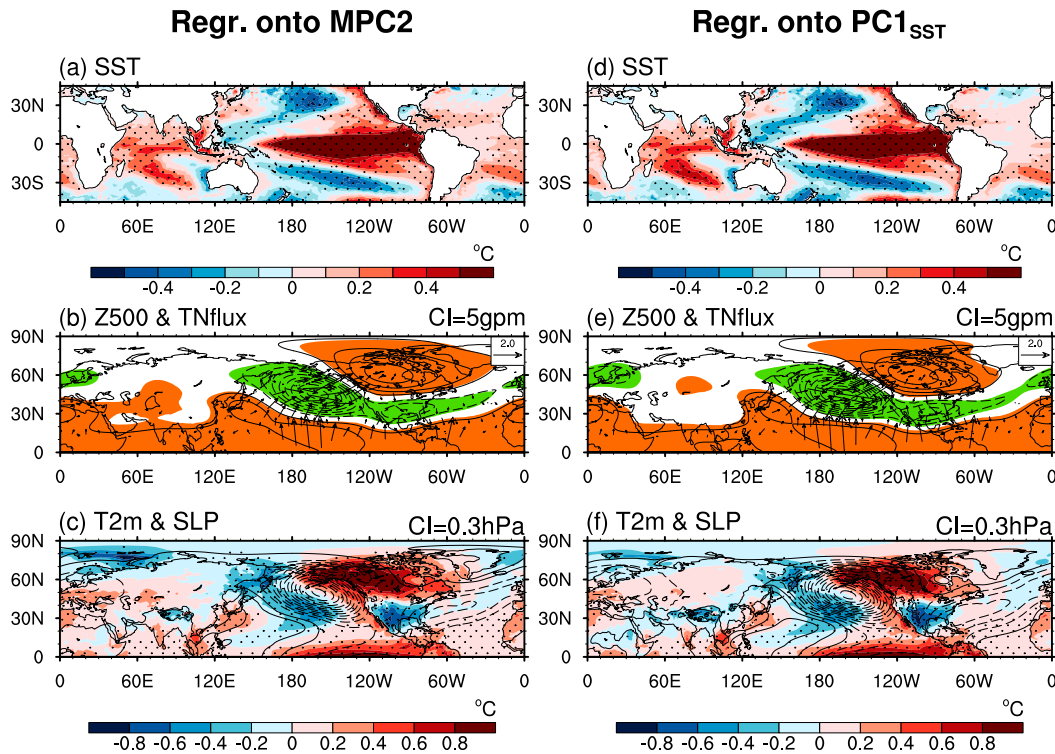


FIG. 4. Regression coefficients of the predicted winter mean (a) SST, (b) 500-hPa geopotential height (contours; CI = 5 gpm) and the associated wave-activity flux (Takaya and Nakamura 2001; arrow;  $\text{m}^2 \text{s}^{-2}$ ), and (c) T2m [shading; shading interval (SI) =  $0.2^\circ\text{C}$ ] and sea level pressure (contours; contour interval = 0.3 hPa) onto the normalized MPC2. (d)–(f) As in (a)–(c), but regressed onto the normalized PC1 of the predicted winter mean SST in the tropical Pacific ( $30^\circ\text{S}$ – $30^\circ\text{N}$ ,  $110^\circ\text{E}$ – $70^\circ\text{W}$ ). Dots in (a), (c), (d), and (f) and shading in (b) and (c) indicate the 5% significance level based on the two-tailed Student's  $t$  test. The arrows whose magnitudes are smaller than  $0.2 \text{ m}^2 \text{ s}^{-2}$  are masked out in (b) and (e).

PNA-like wave train emanating from the subtropical central Pacific (Fig. 5b), which has a rough  $90^\circ$  phase difference from that associated with the MSN EOF2 (Fig. 4b). Linear regression of the predicted SST onto the MPC3 reveals anomalous SST warming in the tropical central Pacific and cooling in the tropical western and eastern Pacific (Fig. 5a), manifesting a CP ENSO pattern (Ashok et al. 2007). These results suggest that the third predictable pattern of T2m likely originates from the SST forcing of the CP ENSO. The CP ENSO is captured by the EOF2 of predicted SST (Fig. 5d), and its associated 500-hPa geopotential height anomalies (Fig. 5e) and T2m anomalies (Fig. 5f) resemble those associated with the MSN EOF3 of T2m over the PNA region (Figs. 5b,c). The correlation coefficient between MPC3 of T2m and PC2 of SST, referred to as  $\text{PC2}_{\text{SST}}$ , is 0.75, exceeding the 1% significance level. These results suggest that the CP ENSO is an essential source of predictability for the T2m's MSN EOF3, especially over the PNA region.

Although the CP ENSO explains the MSN EOF3's source of predictability over the PNA region, it cannot well explain that over the Eurasian continent (Figs. 5c,f), suggesting that other factors should play a role. The MSN EOF3 over Eurasia resembles the leading mode of the Eurasian surface air temperature on the interannual time scale (e.g., Fig. 9a in Wang et al. 2019), which is closely related to the Eurasian snow cover (e.g.,

Allen and Zender 2011). So its possible linkage to the snow cover is examined. Figure 6a shows the predicted winter mean snow depth associated with the MPC3. Reduced snow depth is observed along the Arctic rim of Eurasia to the west of  $130^\circ\text{E}$  and increased snow depth over the rest of Eurasia to the north of approximately  $40^\circ\text{N}$ , with maximum centers over the central Siberian Plateau, surrounding the Altai Mountains, and to the north of the Black Sea, respectively. This pattern is almost identical to the EOF1 of the predicted winter mean snow depth over Eurasia (Fig. 6b). The correlation coefficient between T2m's MPC3 and the PC1 of the predicted winter mean snow depth over Eurasia, referred to as  $\text{PC1}_{\text{snow}}$ , is 0.46, exceeding the 1% significance level. Moreover, the regressed sea level pressure and T2m onto  $\text{PC1}_{\text{snow}}$  (Fig. 6c) quite resemble those associated with the MSN EOF3 (Fig. 5c), although the T2m anomalies over the Ural Mountains region have smaller magnitude (Figs. 5c and 6c). These results suggest that the Eurasian snow cover is an essential source of predictability for the T2m's MSN EOF3 over Eurasia.

#### d. MSN EOF4

Compared with the first three MSN EOFs, the MSN EOF4 explains less variance of T2m over most regions of the Northern Hemisphere except over subtropical Africa and Asia (Fig. 2l), where it accounts for approximately 30% of the

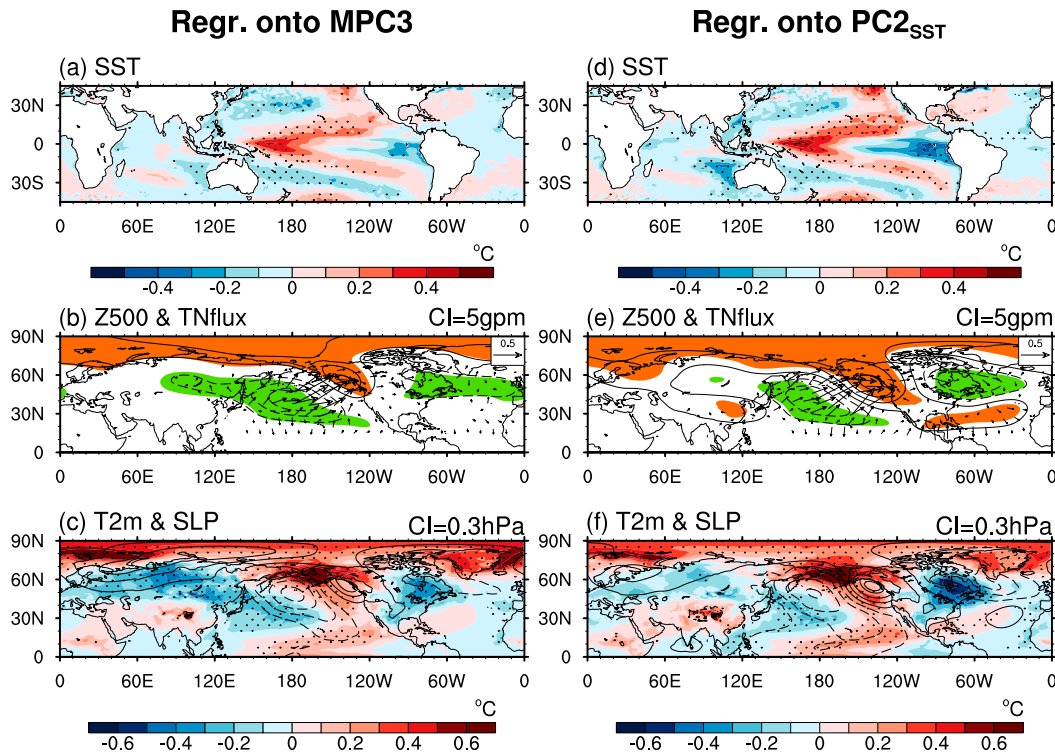


FIG. 5. (a)–(c) As in Figs. 4a–c, but for the MPC3. (d)–(f) As in Figs. 4d–f, but for the PC2 of the SST. The arrows whose magnitudes are smaller than  $0.05 \text{ m}^2 \text{ s}^{-2}$  are masked out in (b) and (e).

variance. It delineates a seesaw-like anomalous T2m pattern, with significant cooling surrounding the Tibetan Plateau and warming over the Barents–Kara Seas (Fig. 7b). This temperature pattern is associated with a midtropospheric wavelike anomaly from the Arctic to the Tibetan Plateau (Fig. 7b), implying its plausible linkage to the Arctic. Inspection of the Arctic sea ice indicates that the MSN EOF4 is closely related to changes in the winter mean SIC over the Barents Sea and Norwegian Sea (Fig. 7a). This MSN EOF4-related SIC pattern is almost identical to the EOF1 of the winter mean SIC over the Arctic ( $70^{\circ}$ – $89^{\circ}$ N) (Fig. 7c). The correlation coefficient between the MPC4 of T2m and the PC1 of the winter mean Arctic SIC, referred to as  $\text{PC1}_{\text{SIC}}$ , is  $-0.51$ , exceeding the 1% significance level. However, the regressed T2m onto  $\text{PC1}_{\text{SIC}}$  (Fig. 7d) shows an opposite sign to that onto the MPC4 surrounding the Tibetan Plateau, although they are quite alike over the Arctic region (Fig. 7b). Note the observed wintertime Arctic and Tibetan T2m vary in phase (e.g., Gu et al. 2018; Zhang et al. 2019), consistent with Fig. 7d, not Fig. 7b. Hence, this result implies the uncertain role of the Arctic SIC in the sources of the predictability for the MSN EOF4.

The cause-and-effect relationship between the Arctic sea ice and the midlatitude climate is complex and has not reached a consensus (Cohen et al. 2020). This complexity is also reflected in the first four MSN EOFs, all of which show similar patterns over the Barents Sea and different patterns over the midlatitudes (Figs. 2a,d,g,j). The correlation coefficients between the

$\text{PC1}_{\text{SIC}}$  and the four MPCs all exceed the 5% significance level (Table 1), and the highest correlation is between  $\text{PC1}_{\text{SIC}}$  and MPC4. This result implies that the plausible forcing of the Arctic sea ice on the wintertime T2m, if any, is most realized through the MSN EOF4 although the MSN EOF4 cannot reproduce the observed Arctic–Tibetan connection of T2m, as discussed in the previous paragraph. Nevertheless, the T2m signals in Figs. 7b and 7d are consistent surrounding the Ural Mountain region. This result suggests that the Arctic SIC may serve as a source of predictability for the T2m variations surrounding the Ural Mountain.

## 5. Improved predictions over Eurasia by incorporating the predictable patterns

It is essential to identify the leading predictable patterns and their sources of predictability because it helps to understand the T2m variability in the SEAS5. It will be practically beneficial if such understanding can be used to improve the prediction skill. To this end, a scheme is developed as an attempt to improve the prediction skill of T2m in the SEAS5. The assumption behind this scheme is that the model can capture the sources of predictability for T2m and that it is incapable of predicting T2m skillfully because it misrepresents the atmospheric responses to these external forcing. Hence, the prediction skill may be improved by incorporating the information related to the leading predictable patterns in a statistical manner. In practice, the prediction is reconstructed based on

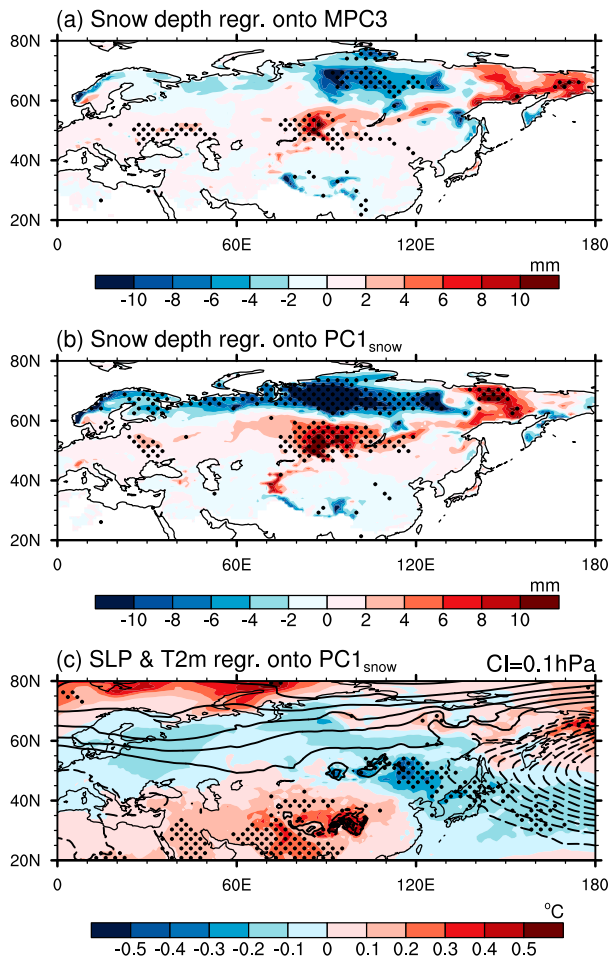


FIG. 6. Regression coefficients of the predicted winter mean snow depth onto the normalized (a) MPC3 and (b) PC1<sub>snow</sub>, the time series of the EOF1 of winter mean snow depth over Eurasia (20°–130°E, 45°–75°N). (c) As in (b), but for the predicted winter mean T2m (shading; shading interval = 0.1°C) and sea level pressure (contours; contour interval = 0.1 hPa). Dots indicate the 5% significance level based on the two-tailed Student's *t* test.

the spatial patterns of leading predictable patterns and time series of the identified predictability sources:

$$\begin{aligned}
 \mathbf{T} &= \sum_{i=1}^4 \mathbf{T}_i \\
 &= \sum_{i=1}^4 \mathbf{e}_i \mathbf{t}_i \\
 &= \mathbf{e}_2^{\text{obs}} \text{MPC1}_{\text{T2m}} + \mathbf{e}_2 \text{PC1}_{\text{SST}} + \mathbf{e}_3 \text{PC1}_{\text{snow}} + \mathbf{e}_4 \text{PC1}_{\text{SIC}}, \quad (5)
 \end{aligned}$$

where  $\mathbf{T}_i$  is the reconstructed T2m prediction based on the *i*th leading predictable pattern  $\mathbf{e}_i$  and the time series of the corresponding predictability source  $\mathbf{t}_i$ . The second to fourth  $\mathbf{e}$  are exactly the spatial patterns of the second to fourth MSN EOFs (Figs. 2d,g,j), and their corresponding  $\mathbf{t}_i$  are the PC1<sub>SST</sub>, PC1<sub>snow</sub>, and PC1<sub>SIC</sub> discussed in sections 4b, 4c, and 4d, respectively. One exception is for  $\mathbf{e}_1$  and  $\mathbf{t}_1$ . Here the spatial

pattern of MSN EOF1 (Fig. 2a) is not used in the reconstruction because it underestimates the warming trend over the Arctic and misses the cooling trend over Eurasia (Fig. 3c). Instead, the observed EOF2 of the extratropical wintertime T2m ( $\mathbf{e}_2^{\text{obs}}$ ; Fig. 3d) is used. The  $\mathbf{e}_2^{\text{obs}}$ , not the pattern of T2m's trend (Fig. 3b), is used for the easier extracting patterns in cross-validation. More importantly, the  $\mathbf{e}_2^{\text{obs}}$  can well represent the observed pattern of T2m's trend (Fig. 3b), and its time series is highly correlated ( $r = 0.92$ ) to that of the observed T2m's trend, which is obtained by projecting the observed T2m onto the observed T2m's trend (Fig. 3b). Here  $\mathbf{t}_1$  equals MPC1<sub>T2m</sub> that is obtained by projecting the MSN EOF1 onto the predicted T2m over the extratropical Northern Hemisphere (20°–89°N). The use of MPC1<sub>T2m</sub> guarantees that the time series of  $\mathbf{t}_1$  can be generated within the model for the prediction purpose, although the spatial pattern is replaced by the observation ( $\mathbf{e}_2^{\text{obs}}$ ). The PC2<sub>SST</sub> was not used to replace  $\mathbf{t}_3$  because the focus is on Eurasia, where the prediction skill is low (Fig. 1a), and the influence of the CP ENSO is relatively weak (Fig. 5f). The amplitudes of  $\mathbf{t}_i$  are adjusted prior to the reconstruction to match their substitutes using the standard deviations of the substitutes.

To test the capability of the calibration scheme, the leave-one-out cross-validation method (Michaelsen 1987) was employed. This method reconstructs the wintertime T2m in a specific year based on the remaining years other than this year using the forecast model in Eq. (5). For example, the MSN EOF and EOF analyses are performed during the years 1981–90 combined with 1992–2016, and the resultant information is used to reconstruct the T2m in the year 1991. The above approaches are repeated so that T2m in every year during 1981–2016 is reconstructed. Figure 8a shows the ACC between observed and reconstructed T2m using the first four MSN EOFs in the leave-one-out cross-validation. The ACC generally exceeds 0.3 over large areas of midlatitude Eurasia. This performance is in sharp contrast to the low and even negative ACC based on the ensemble mean of direct model outputs in this region (Fig. 1a). It suggests that the reconstructed T2m shows apparent improvement in the prediction skill over midlatitude Eurasia (e.g., between 45° and 70°N) compared with the direct ensemble mean of the SEAS5, especially in regions to the east of Ural Mountains (Fig. 8b). The improvement of the ACC (Fig. 8b) projects well onto the pattern of the MSN EOF3 (Fig. 2g) and  $\mathbf{e}_2^{\text{obs}}$  (Fig. 3d), implying its primary origins from the Eurasian snow cover and the warm Arctic–cold continent pattern. Inspection of the effects of individual factors on the ACC confirms this inference (Fig. 9). Meanwhile, it is noteworthy that the prediction skill of reconstructed T2m is worse than the direct ensemble means of the SEAS5 in most of the Northern Hemisphere other than Eurasia. On the one hand, this result is understandable because the performance of the SEAS5 is already good in regions outside Eurasia. It is insufficient to use only four predictable modes for the reconstruction in these regions. On the other hand, this result suggests that it is very likely an efficient way to replace the model predicted T2m with reconstructed T2m over midlatitude Eurasia to improve the prediction skill of wintertime T2m in the SEAS5.

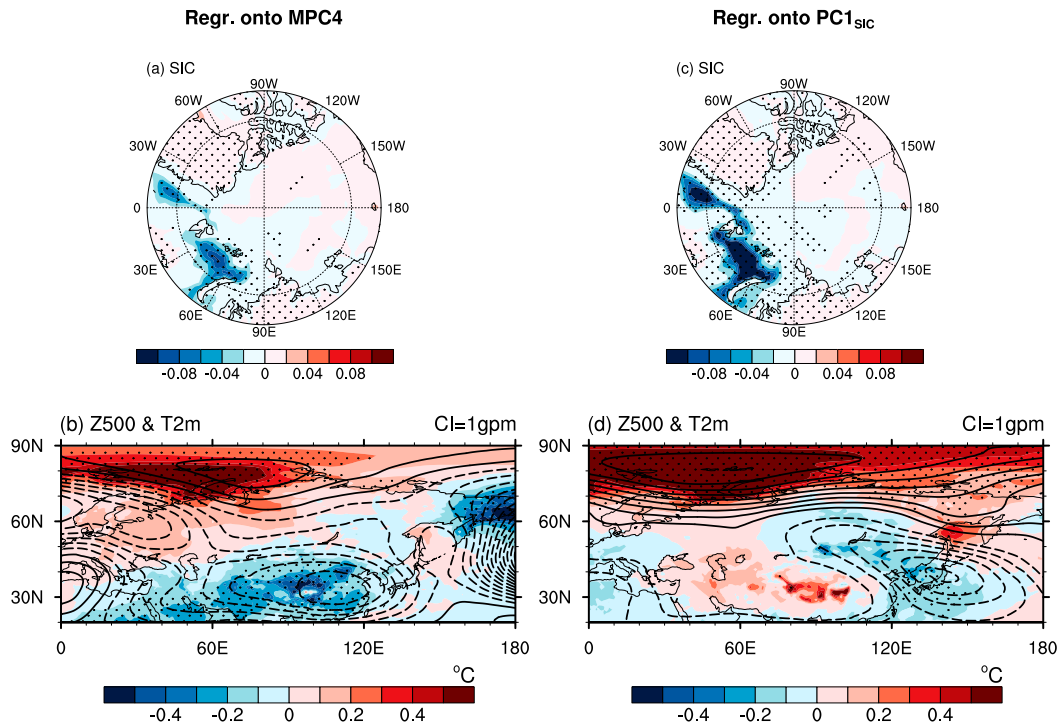


FIG. 7. Regression coefficients of the predicted winter mean (a) SIC and (b) T2m (shading; shading interval = 0.02) and 500-hPa geopotential height (contour; contour interval = 1 gpm) onto the normalized MPC4. (c),(d) As in (a) and (b), but regressed onto the normalized PC1 of the predicted winter mean SIC in the Arctic (70°–89°N). Dots indicate the 5% significance level of the (top) SIC and (bottom) T2m based on the two-tailed Student's  $t$  test. The regression coefficients in (c) and (d) have been multiplied by  $-1$  for the convenience of comparison.

## 6. Conclusions and discussion

Slow-varying atmospheric boundaries are the main sources of seasonal climate predictions, and their footprints on climate variables may be captured as predictable patterns. Based on the 36-yr hindcast data from the SEAS5, the latest ECMWF seasonal forecast system, this study extracted the leading predictable patterns of the extratropical Northern Hemisphere T2m in boreal winter via the MSN EOF analysis and identified their sources of predictability. The MSN EOF1, the dominant predictable pattern, explains 53.2% of the total variance and reflects the long-term warming trend of T2m. The SEAS5 underestimates the observed magnitude of the warming trend and misses the observed warm Arctic–cold continent pattern. The MSN EOF2 and MSN EOF3, which explain 15.9% and 9.3% of the total variance, respectively, manifest a wavelike T2m pattern over the PNA region. Their sources of predictability can be traced to the tropical forcing associated with the EP and CP ENSO, respectively. In addition, the MSN EOF3 has large loading over the midlatitude Eurasia that cannot be explained by the CP ENSO. Inspection suggests that this T2m variability over Eurasia can be attributed to the forcing from the Eurasian snow. The MSN EOF4 explains only 5.1% of the total variance, and it delineates T2m variability surrounding the Tibetan Plateau. Its source of predictability can be partially traced to the Arctic sea ice in the Barents and Norwegian Seas with some uncertainty. The SEAS5's prediction skill of the

wintertime T2m is overall good in the extratropical Northern Hemisphere except over midlatitude Eurasia. A calibration scheme is developed as an attempt to improve the prediction skill of T2m by reinforcing the information of the first four MSN EOFs and their sources of predictability. It reveals that the prediction skill in terms of the ACC improves significantly over midlatitude Eurasia in a leave-one-out cross-validation. This result confirms the importance of the predictable patterns and their sources in the seasonal predictions and implies a possible way to improve the wintertime T2m prediction over Eurasia.

In this study, the wintertime atmospheric external forcing was identified as a source of predictability for the leading predictable patterns. This approach is usually acceptable for remote forcing such as that from ENSO, but it may be questioned for the in situ atmospheric boundaries such as midlatitude snow cover and sea ice because of their strong interactions with the atmosphere. On the one hand, such questions are reasonable to some extent because there are

TABLE 1. Correlation coefficients between the predicted PC1<sub>SIC</sub> and the four MPCs during winters 1981–2016. Values exceeding the 5% and 1% significance levels based on the two-tailed Student's  $t$  test are denoted by one and two asterisks, respectively (\* and \*\*).

	MPC1	MPC2	MPC3	MPC4
PC1 <sub>SIC</sub>	−0.40*	0.33*	−0.40*	−0.51**

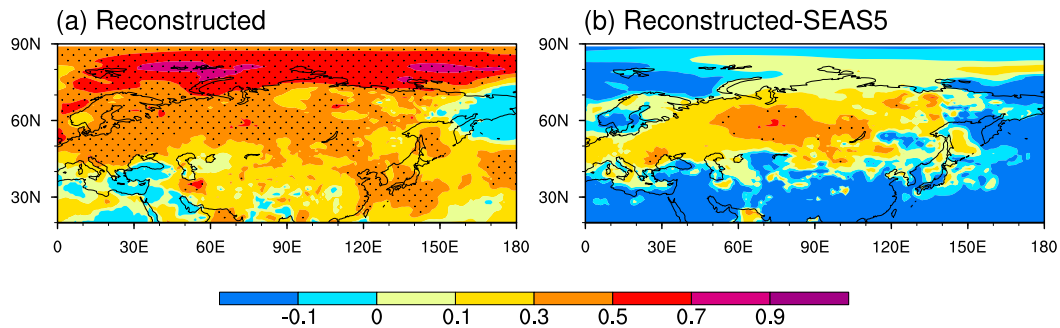


FIG. 8. (a) The prediction skill of reconstructed T2m using the first four MSN EOFs measured by the ACC between observed T2m and reconstructed T2m. See text for details of the reconstruction. (b) The difference of ACC between reconstructed T2m prediction skill (Fig. 8a) and direct T2m prediction skill in the SEAS5 (Fig. 2a). Dots indicate the 5% and 10% significance level based on the two-tailed Student's  $t$  test in (a) and (b), respectively.

indeed interactions between the extratropical atmosphere and the underlying snow cover or sea ice. Strictly speaking, the signals of wintertime Eurasia snow cover and Arctic sea ice used in this study are the results of these interactions. On the other hand, it is reasonable to regard these wintertime signals as relative external forcing because they indeed force the atmosphere in the interaction with the atmosphere. As a result, reconstructed T2m by incorporating these forcing signals improves the prediction skill significantly over Eurasia. Nevertheless, it is noteworthy that the SEAS5 is a coupled model that does not have boundary forcing. Hence, the identified atmospheric external forcing and, thereby, the predictability sources should finally be from initial fields of long memory. It is meaningful to track these initial

conditions for the predictable patterns, but it cannot be done in this study because of the unavailability of related data. Last but not least, this study is based on the SEAS5. It would be meaningful to examine the robustness of the results in other seasonal forecast systems, and this will be done in the future.

*Acknowledgments.* We thank the three anonymous reviewers for their valuable comments and suggestions. This work was supported by the National Key R&D Program of China (2018YFC1506001) and the National Natural Science Foundation of China (41925020, 41721004). We thank Dr. Lijuan Hua for providing literature on significance tests on linear trends.

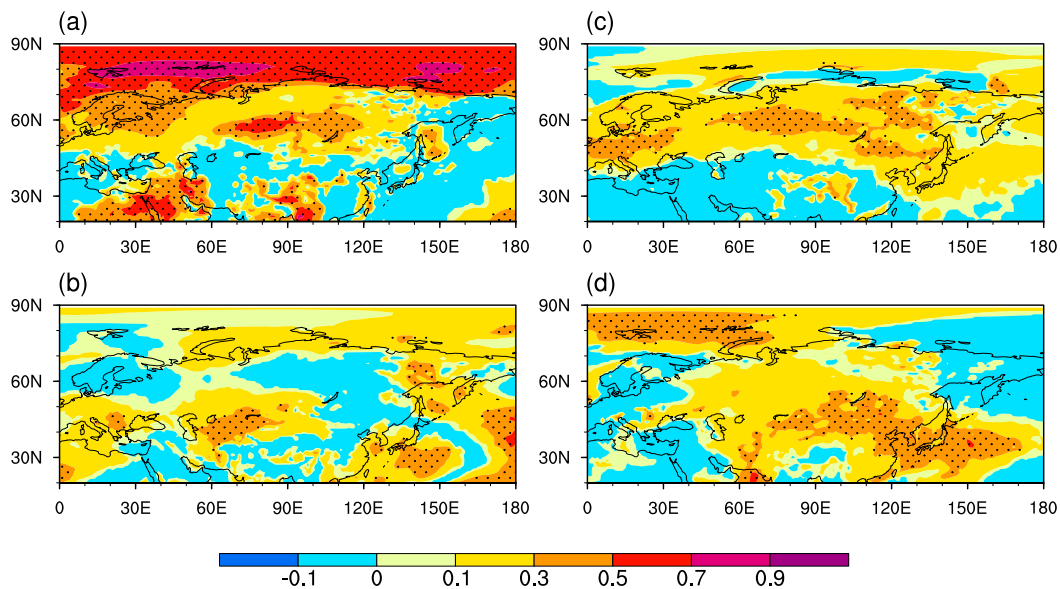


FIG. 9. The ACC between observed T2m and reconstructed T2m using the (a) first, (b) second, (c) third, and (d) fourth MSN EOF alone. Dots indicate the 5% significance level based on the two-tailed Student's  $t$  test.

## REFERENCES

- Allen, M. R., and L. A. Smith, 1997: Optimal filtering in singular spectrum analysis. *Phys. Lett.*, **234A**, 419–428, [https://doi.org/10.1016/S0375-9601\(97\)00559-8](https://doi.org/10.1016/S0375-9601(97)00559-8).
- Allen, R. J., and C. S. Zender, 2011: Forcing of the Arctic Oscillation by Eurasian snow cover. *J. Climate*, **24**, 6528–6539, <https://doi.org/10.1175/2011JCLI4157.1>.
- Ashok, K., S. K. Behera, S. A. Rao, H. Weng, and T. Yamagata, 2007: El Niño Modoki and its possible teleconnection. *J. Geophys. Res.*, **112**, C11007, <https://doi.org/10.1029/2006JC003798>.
- Bauer, P., A. Thorpe, and G. Brunet, 2015: The quiet revolution of numerical weather prediction. *Nature*, **525**, 47–55, <https://doi.org/10.1038/nature14956>.
- Brönnimann, S., 2007: Impact of El Niño–Southern Oscillation on European climate. *Rev. Geophys.*, **45**, RG3003, <https://doi.org/10.1029/2006RG000199>.
- Charney, J. G., and J. Shukla, 1981: Predictability of monsoons. *Monsoon Dynamics*, J. Lighthill and R. P. Pearce, Eds., Cambridge University Press, 99–109.
- Chen, W., J. Feng, and R. Wu, 2013: Roles of ENSO and PDO in the link of the East Asian winter monsoon to the following summer monsoon. *J. Climate*, **26**, 622–635, <https://doi.org/10.1175/JCLI-D-12-00021.1>.
- Chylek, P., C. K. Folland, G. Lesins, M. K. Dubey, and M. Wang, 2009: Arctic air temperature change amplification and the Atlantic multidecadal oscillation. *Geophys. Res. Lett.*, **36**, L14801, <https://doi.org/10.1029/2009GL038777>.
- Cohen, J., and C. Fletcher, 2007: Improved skill of Northern Hemisphere winter surface temperature predictions based on land–atmosphere fall anomalies. *J. Climate*, **20**, 4118–4132, <https://doi.org/10.1175/JCLI4241.1>.
- , J. C. Furtado, M. Barlow, V. A. Alexeev, and J. E. Cherry, 2012: Asymmetric seasonal temperature trends. *Geophys. Res. Lett.*, **39**, L04705, <https://doi.org/10.1029/2011GL050582>.
- , and Coauthors, 2014: Recent Arctic amplification and extreme mid-latitude weather. *Nat. Geosci.*, **7**, 627–637, <https://doi.org/10.1038/ngeo2234>.
- , and Coauthors, 2020: Divergent consensus on Arctic amplification influence on midlatitude severe winter weather. *Nat. Climate Change*, **10**, 20–29, <https://doi.org/10.1038/s41558-019-0662-y>.
- Conlon, M., and R. G. Thomas, 1993: The power function for Fisher's exact test. *J. Roy. Stat. Soc.*, **42C**, 258–260, <https://doi.org/10.2307/2347431>.
- Dee, D. P., and Coauthors, 2011: The ERA-Interim reanalysis: Configuration and performance of the data assimilation system. *Quart. J. Roy. Meteor. Soc.*, **137**, 553–597, <https://doi.org/10.1002/qj.828>.
- DelSole, T., and M. K. Tippett, 2007: Predictability: Recent insights from information theory. *Rev. Geophys.*, **45**, RG4002, <https://doi.org/10.1029/2006RG000202>.
- Ding, Q., J. M. Wallace, D. S. Battisti, E. J. Steig, A. J. Gallant, H. J. Kim, and L. Geng, 2014: Tropical forcing of the recent rapid Arctic warming in northeastern Canada and Greenland. *Nature*, **509**, 209–212, <https://doi.org/10.1038/nature13260>.
- Doblas-Reyes, F. J., J. García-Serrano, F. Lienert, A. P. Biescas, and L. R. L. Rodrigues, 2013: Seasonal climate predictability and forecasting: Status and prospects. *Wiley Interdiscip. Rev.: Climate Change*, **4**, 245–268, <https://doi.org/10.1002/wcc.217>.
- Gong, H., L. Wang, and W. Chen, 2019: Recently strengthened influence of ENSO on the wintertime East Asian surface air temperature. *Atmosphere*, **10**, 720, <https://doi.org/10.3390/atmos10110720>.
- Graversen, R. G., T. Mauritsen, M. Tjernstrom, E. Kallen, and G. Svensson, 2008: Vertical structure of recent Arctic warming. *Nature*, **451**, 53–56, <https://doi.org/10.1038/nature06502>.
- Gu, G. J., and R. F. Adler, 2019: Precipitation, temperature, and moisture transport variations associated with two distinct ENSO flavors during 1979–2014. *Climate Dyn.*, **52**, 7249–7265, <https://doi.org/10.1007/s00382-016-3462-3>.
- Gu, S., Y. Zhang, Q. Wu, and X.-Q. Yang, 2018: The linkage between Arctic sea ice and midlatitude weather: In the perspective of energy. *J. Geophys. Res. Atmos.*, **123**, 11 536–11 550, <https://doi.org/10.1029/2018JD028743>.
- Horel, J. D., and J. M. Wallace, 1981: Planetary-scale atmospheric phenomena associated with the Southern Oscillation. *Mon. Wea. Rev.*, **109**, 813–829, [https://doi.org/10.1175/1520-0493\(1981\)109<0813:PSAPAW>2.0.CO;2](https://doi.org/10.1175/1520-0493(1981)109<0813:PSAPAW>2.0.CO;2).
- Huang, B., 2004: Remotely forced variability in the tropical Atlantic Ocean. *Climate Dyn.*, **23**, 133–152, <https://doi.org/10.1007/s00382-004-0443-8>.
- Ineson, S., and A. A. Scaife, 2008: The role of the stratosphere in the European climate response to El Niño. *Nat. Geosci.*, **2**, 32–36, <https://doi.org/10.1038/ngeo381>.
- Jia, L., and Coauthors, 2017: Seasonal prediction skill of northern extratropical surface temperature driven by the stratosphere. *J. Climate*, **30**, 4463–4475, <https://doi.org/10.1175/JCLI-D-16-0475.1>.
- Johnson, S. J., and Coauthors, 2019: SEAS5: The new ECMWF seasonal forecast system. *Geosci. Model Dev.*, **12**, 1087–1117, <https://doi.org/10.5194/gmd-12-1087-2019>.
- Kim, H.-M., P. J. Webster, and J. A. Curry, 2012: Seasonal prediction skill of ECMWF system 4 and NCEP CFSv2 retrospective forecast for the Northern Hemisphere winter. *Climate Dyn.*, **39**, 2957–2973, <https://doi.org/10.1007/s00382-012-1364-6>.
- Kumar, K. K., B. Rajagopalan, and M. A. Cane, 1999: On the weakening relationship between the Indian monsoon and ENSO. *Science*, **284**, 2156–2159, <https://doi.org/10.1126/science.284.5423.2156>.
- Liang, J., S. Yang, Z.-Z. Hu, B. Huang, A. Kumar, and Z. Zhang, 2008: Predictable patterns of the Asian and Indo-Pacific summer precipitation in the NCEP CFS. *Climate Dyn.*, **32**, 989–1001, <https://doi.org/10.1007/s00382-008-0420-8>.
- Lorenz, E. N., 1963: Deterministic nonperiodic flow. *J. Atmos. Sci.*, **20**, 130–141, [https://doi.org/10.1175/1520-0469\(1963\)020<0130:DNF>2.0.CO;2](https://doi.org/10.1175/1520-0469(1963)020<0130:DNF>2.0.CO;2).
- Michaelsen, J., 1987: Cross-validation in statistical climate forecast models. *J. Climate Appl. Meteor.*, **26**, 1589–1600, [https://doi.org/10.1175/1520-0450\(1987\)026<1589:CVISCF>2.0.CO;2](https://doi.org/10.1175/1520-0450(1987)026<1589:CVISCF>2.0.CO;2).
- North, G. R., T. L. Bell, R. F. Cahalan, and F. J. Moeng, 1982: Sampling errors in the estimation of empirical orthogonal functions. *Mon. Wea. Rev.*, **110**, 699–706, [https://doi.org/10.1175/1520-0493\(1982\)110<0699:SEITEO>2.0.CO;2](https://doi.org/10.1175/1520-0493(1982)110<0699:SEITEO>2.0.CO;2).
- Overland, J. E., K. R. Wood, and M. Wang, 2011: Warm Arctic–cold continents: Climate impacts of the newly open Arctic Sea. *Polar Res.*, **30**, 15 787, <https://doi.org/10.3402/polar.v30i0.15787>.
- Palmer, T. N., 1993: Extended-range atmospheric prediction and the Lorenz model. *Bull. Amer. Meteor. Soc.*, **74**, 49–65, [https://doi.org/10.1175/1520-0477\(1993\)074<0049:ERAPAT>2.0.CO;2](https://doi.org/10.1175/1520-0477(1993)074<0049:ERAPAT>2.0.CO;2).
- Rayner, N. A., D. E. Parker, E. B. Horton, C. K. Folland, L. V. Alexander, D. P. Rowell, E. C. Kent, and A. Kaplan, 2003: Global analyses of sea surface temperature, sea ice, and night marine air temperature since the late nineteenth century. *J. Geophys. Res.*, **108**, 4407, <https://doi.org/10.1029/2002JD002670>.
- Rowell, D. P., 1998: Assessing potential seasonal predictability with an ensemble of multidecadal GCM simulations. *J. Climate*, **11**, 109–120, [https://doi.org/10.1175/1520-0442\(1998\)011<0109:APSPA>2.0.CO;2](https://doi.org/10.1175/1520-0442(1998)011<0109:APSPA>2.0.CO;2).

- Santer, B. D., T. M. L. Wigley, J. S. Boyle, D. J. Gaffen, J. J. Hnilo, D. Nychka, D. E. Parker, and K. E. Taylor, 2000: Statistical significance of trends and trend differences in layer-average atmospheric temperature time series. *J. Geophys. Res.*, **105**, 7337–7356, <https://doi.org/10.1029/1999JD901105>.
- Simmons, A. J., and A. Hollingsworth, 2002: Some aspects of the improvement in skill of numerical weather prediction. *Quart. J. Roy. Meteor. Soc.*, **128**, 647–677, <https://doi.org/10.1256/003590002321042135>.
- Stocker, T. F., and Coauthors, 2013: Technical summary. *Climate Change 2013: The Physical Science Basis*, T. F. Stocker et al., Eds., Cambridge University Press, 33–115.
- Takaya, K., and H. Nakamura, 2001: A formulation of a phase-independent wave-activity flux for stationary and migratory quasi-geostrophic eddies on a zonally varying basic flow. *J. Atmos. Sci.*, **58**, 608–627, [https://doi.org/10.1175/1520-0469\(2001\)058<0608:AFOAPI>2.0.CO;2](https://doi.org/10.1175/1520-0469(2001)058<0608:AFOAPI>2.0.CO;2).
- Tang, Y., D. Chen, and X. Yan, 2014: Potential predictability of North American surface temperature. Part I: Information-based versus signal-to-noise-based metrics. *J. Climate*, **27**, 1578–1599, <https://doi.org/10.1175/JCLI-D-12-00654.1>.
- , —, and —, 2015: Potential predictability of Northern America surface temperature in AGCMs and CGCMs. *Climate Dyn.*, **45**, 353–374, <https://doi.org/10.1007/s00382-014-2335-x>.
- Wang, L., W. Chen, and R. H. Huang, 2007: Changes in the variability of North Pacific Oscillation around 1975/76 and its relationship with East Asian winter climate. *J. Geophys. Res.*, **112**, D11110, <https://doi.org/10.1029/2006JD008054>.
- , —, and R. Huang, 2008: Interdecadal modulation of PDO on the impact of ENSO on the East Asian winter monsoon. *Geophys. Res. Lett.*, **35**, L20702, <https://doi.org/10.1029/2008GL035287>.
- , A. Deng, and R. Huang, 2019: Wintertime internal climate variability over Eurasia in the CESM large ensemble. *Climate Dyn.*, **52**, 6735–6748, <https://doi.org/10.1007/s00382-018-4542-3>.
- Wu, R. G., and B. Wang, 2002: A contrast of the East Asian summer monsoon–ENSO relationship between 1962–77 and 1978–93. *J. Climate*, **15**, 3266–3279, [https://doi.org/10.1175/1520-0442\(2002\)015<3266:ACOTEA>2.0.CO;2](https://doi.org/10.1175/1520-0442(2002)015<3266:ACOTEA>2.0.CO;2).
- Wu, Y., and Y. Tang, 2019: Seasonal predictability of the tropical Indian Ocean SST in the North American multimodel ensemble. *Climate Dyn.*, **53**, 3361–3372, <https://doi.org/10.1007/s00382-019-04709-0>.
- Xie, S.-P., Y. Kosaka, Y. Du, K. Hu, J. S. Chowdary, and G. Huang, 2016: Indo-western Pacific Ocean capacitor and coherent climate anomalies in post-ENSO summer: A review. *Adv. Atmos. Sci.*, **33**, 411–432, <https://doi.org/10.1007/s00376-015-5192-6>.
- Zhang, Y., T. Zou, and Y. Xue, 2019: An Arctic–Tibetan connection on subseasonal to seasonal time scale. *Geophys. Res. Lett.*, **46**, 2790–2799, <https://doi.org/10.1029/2018GL081476>.
- Zhu, J., B. Huang, Z.-Z. Hu, J. L. Kinter III, and L. Marx, 2013: Predicting US summer precipitation using NCEP Climate Forecast System version 2 initialized by multiple ocean analyses. *Climate Dyn.*, **41**, 1941–1954, <https://doi.org/10.1007/s00382-013-1785-x>.
- , —, A. Kumar, and J. L. Kinter III, 2015: Seasonality in prediction skill and predictable pattern of tropical Indian Ocean SST. *J. Climate*, **28**, 7962–7984, <https://doi.org/10.1175/JCLI-D-15-0067.1>.
- , A. Kumar, H. C. Lee, and H. Wang, 2017: Seasonal predictions using a simple ocean initialization scheme. *Climate Dyn.*, **49**, 3989–4007, <https://doi.org/10.1007/s00382-017-3556-6>.
- Zuo, Z., S. Yang, W. Wang, A. Kumar, Y. Xue, and R. Zhang, 2011: Relationship between anomalies of Eurasian snow and southern China rainfall in winter. *Environ. Res. Lett.*, **6**, 045402, <https://doi.org/10.1088/1748-9326/6/4/045402>.
- , —, Z.-Z. Hu, R. Zhang, W. Wang, B. Huang, and F. Wang, 2013: Predictable patterns and prediction skills of monsoon precipitation in Northern Hemisphere summer in NCEP CFSv2 reforecasts. *Climate Dyn.*, **40**, 3071–3088, <https://doi.org/10.1007/s00382-013-1772-2>.
- , —, R. Zhang, D. Xiao, D. Guo, and L. Ma, 2015: Response of summer rainfall over China to spring snow anomalies over Siberia in the NCEP CFSv2 reforecast. *Quart. J. Roy. Meteor. Soc.*, **141**, 939–944, <https://doi.org/10.1002/qj.2413>.